Fig.  $\alpha'$ 

Inelastic population of the  $11\text{Be}(5/2^+; 1.45 \text{ MeV})$  theoretically calculated resonance. (a) Process dressing the neutron moving in the  $5/2^-$  orbital and leading to the  $11\text{Be}$  ground state. The virtual state is made out of the fully renormalized (real, empirical) quadrupole vibration of the core  $10\text{Be}$  and of the low-lying  $5/2^+$  resonance of  $11\text{Be}$ , and is indicated by using bold face symbols.  
 (b) Intervening process (a) with an external inelastic hadron field (e.g.,  $(p, p')$ ) of quadrupole character (dashed horizontal line ~~ending~~<sup>starting</sup> at cross), or can excite the  $5/2^+$  resonance. This can also happen if the external field acts on the  $1/2^+$  state as in (c), or if this field excites the quadrupole vibration of the  $10\text{Be}$  which eventually couple to the  $1/2^+$  state as in (d). (e) If the vibration was a high-lying quadrupole grant resonance the summed contribution of processes (b)-(d) could be replaced at profit

København 17/08/17.

(F2)

(14)

by a single graph, namely the equivalent  
of (c) but with an effective charge, hatched  
circle. For low-lying modes like the 3.368 MeV  
quadrupole vibration of  $^{10}\text{Be}$ , ~~the~~ retardation,  
 $\omega$ -dependent effect have to be  
explicitly taken into account.

(15)

 crossed rectangle  $\gamma$ -detector

 hatched rectangle particle detector

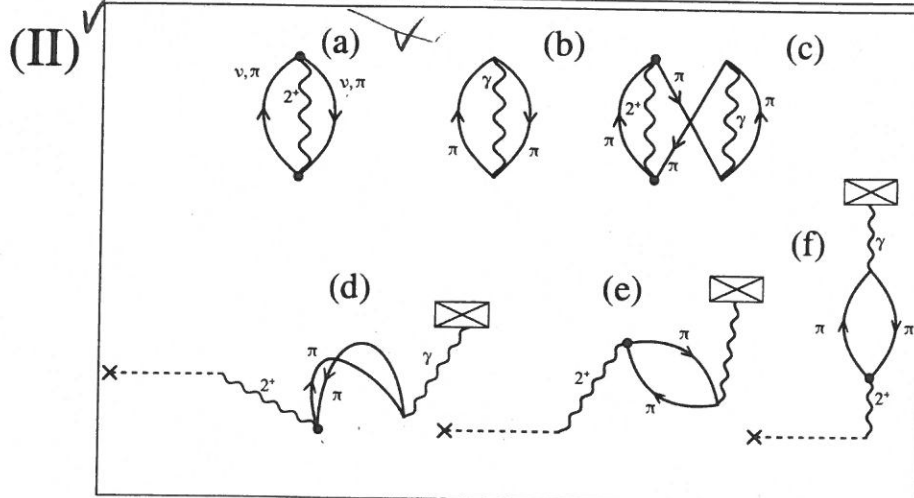
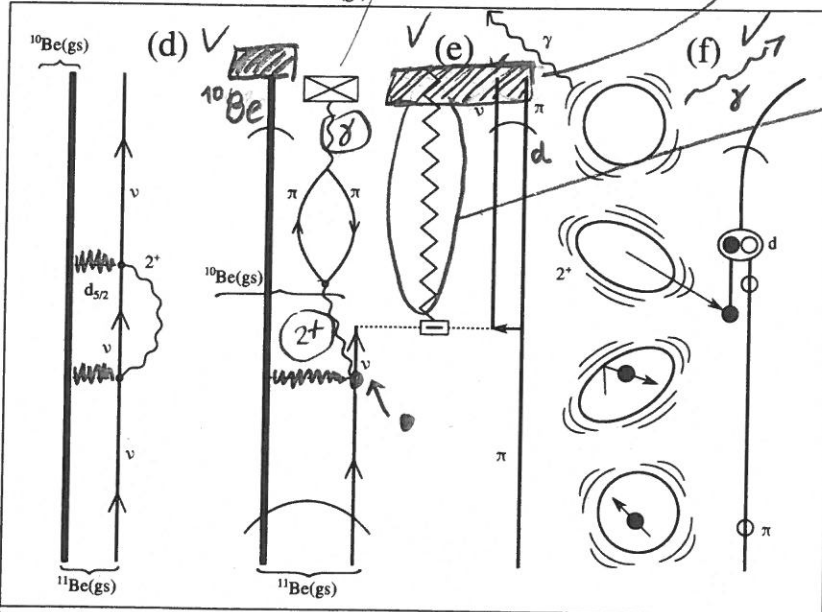
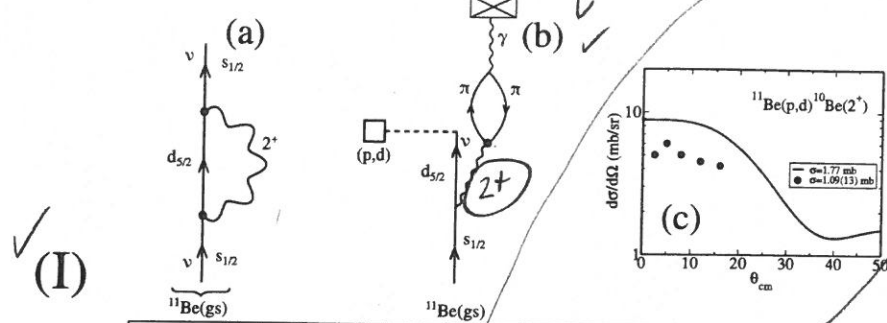


FIG. 3 ✓

Fig. a

Caption to Fig. 3

*Caption to Fig. 2 (paper Hawking  
Fig. 3)*

(I) A virtual process in nuclear physics becomes real through the action of an external field. (a) Clothing process of the  $1/2^+$  parity inverted ground state of  $^{11}_4\text{Be}_7$  through the coupling to the low-lying quadrupole vibration of the core  $^{10}_4\text{Be}_6$ ; (b) schematic representation of the pickup of the neutron moving around a  $N = 6$  closed shell and populating the low-lying quadrupole vibrational state of this core, in coincidence with the corresponding  $\gamma$ -decay (see also II (f)); the detailed structure and reaction NFT diagram describing the pickup process in inverse kinematics, i.e.  ${}^1\text{H}({}^{11}\text{Be}, {}^{10}\text{Be}(2^+, 3.368 \text{ MeV})) {}^2\text{He}$  is shown in (d) and (e) together with a cartoon representation in (f) (the jagged line represents a graphic mnemonic of the recoil effect, see [8] App. F as well as [29], App. A). Proton and neutrons are labeled  $\pi$  and  $\nu$  respectively, while  $d$  stands for deuteron. Curved arrows indicate projectile motion (reaction). Normal arrowed lines, motion inside target or projectile (structure); (c) predicted (continuous curve) and experimental (solid dots) absolute differential cross sections associated with the indicated pickup process. (II) Interaction of protons in a nucleus with nuclear vibrations (solid dot, PVC vertex  $\beta_L R_0 \partial U / \partial r Y_{LM}^*(\hat{r})$ ,  $\beta_L$ : dynamical distortion parameter,  $U(r)$  central potential) and photons (normal vertex, see also Fig. 1(I)(a), electromagnetic interaction  $e \int d^4x J_\mu(x) A^\mu(x)$ ,  $A^\mu$  being the vector potential, and  $J_\mu$  the current density ( $\mu = 1, \dots, 4$ )). While the variety of diagrams shown have general validity, we have assumed we are dealing with the low-lying correlated particle-hole quadrupole vibration ( $L = 2$ ) of  $^{10}_4\text{Be}_6$  lying at 3.368 MeV,  $B(E2; 0^+ \rightarrow 2^+) = 0.0052 e^2 b^2$  being associated with  $\beta_2 \approx 0.9$ . An arrowed line pointing upward (downward) describes a proton (proton hole) moving in the  $p_{1/2}$  ( $1p_{3/2}$ ) orbital. Zero point fluctuations of the nuclear ground state associated with: (a) the nuclear vibration, (b) the electromagnetic field associated with the corresponding spontaneous  $\gamma$ -decay. (c) Pauli principle correction to the simultaneous presence of the above two ZPF processes. (d) Intervening the virtual excitation of the nuclear vibrations (graph (c)) with an external (inelastic) field (cross followed by a dashed line), in coincidence with the  $\gamma$ -decay ( $\gamma$ -detector, crossed box), the virtual process (c) becomes real. (e), (f) time ordering of the above process correspond to the RPA contributions through backwardsgoing and forwardsgoing amplitudes and subsequent  $\gamma$ -decay.

Particle  
detectors  
are drawn  
as hatched  
rectangles

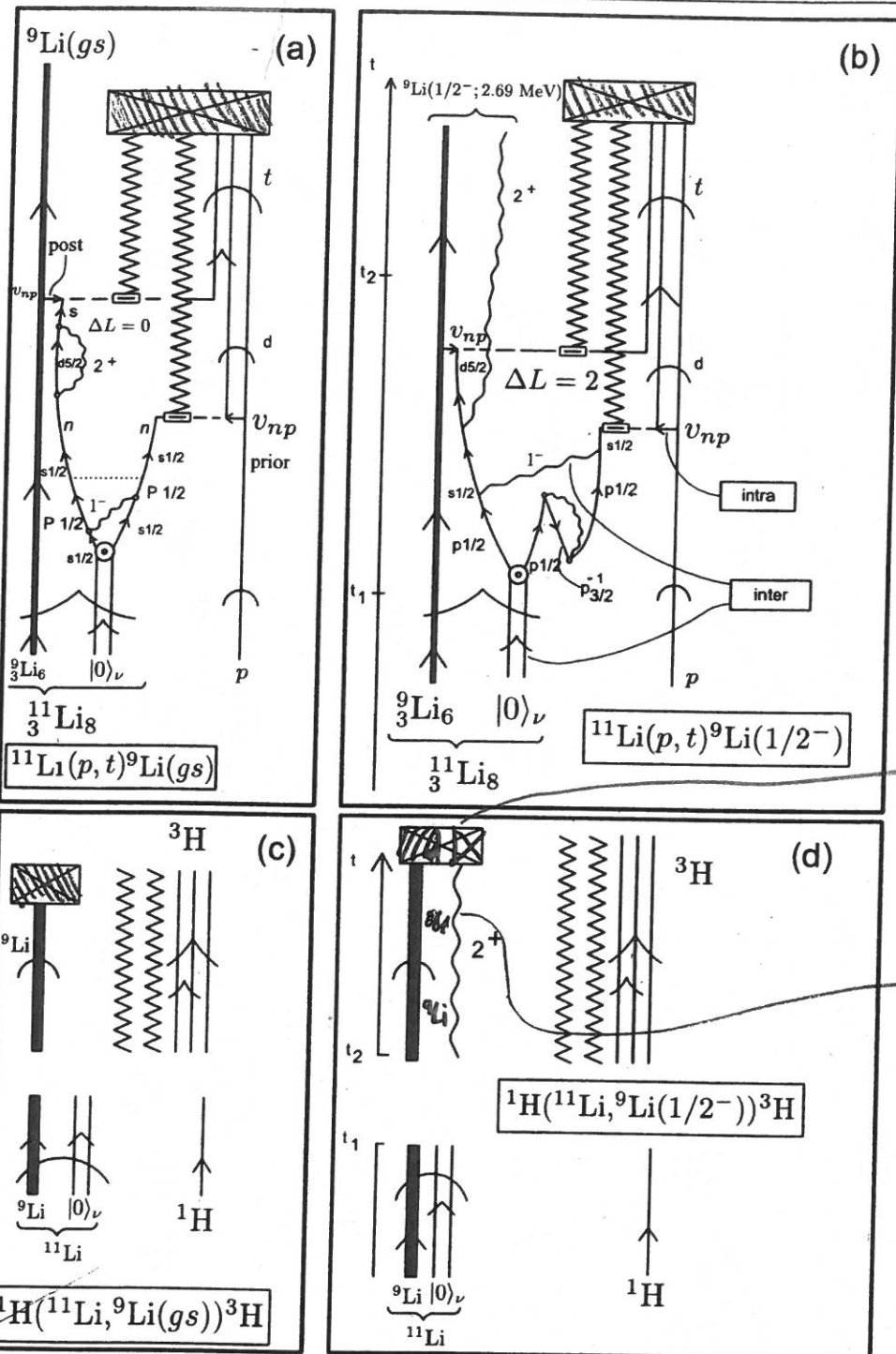
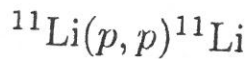


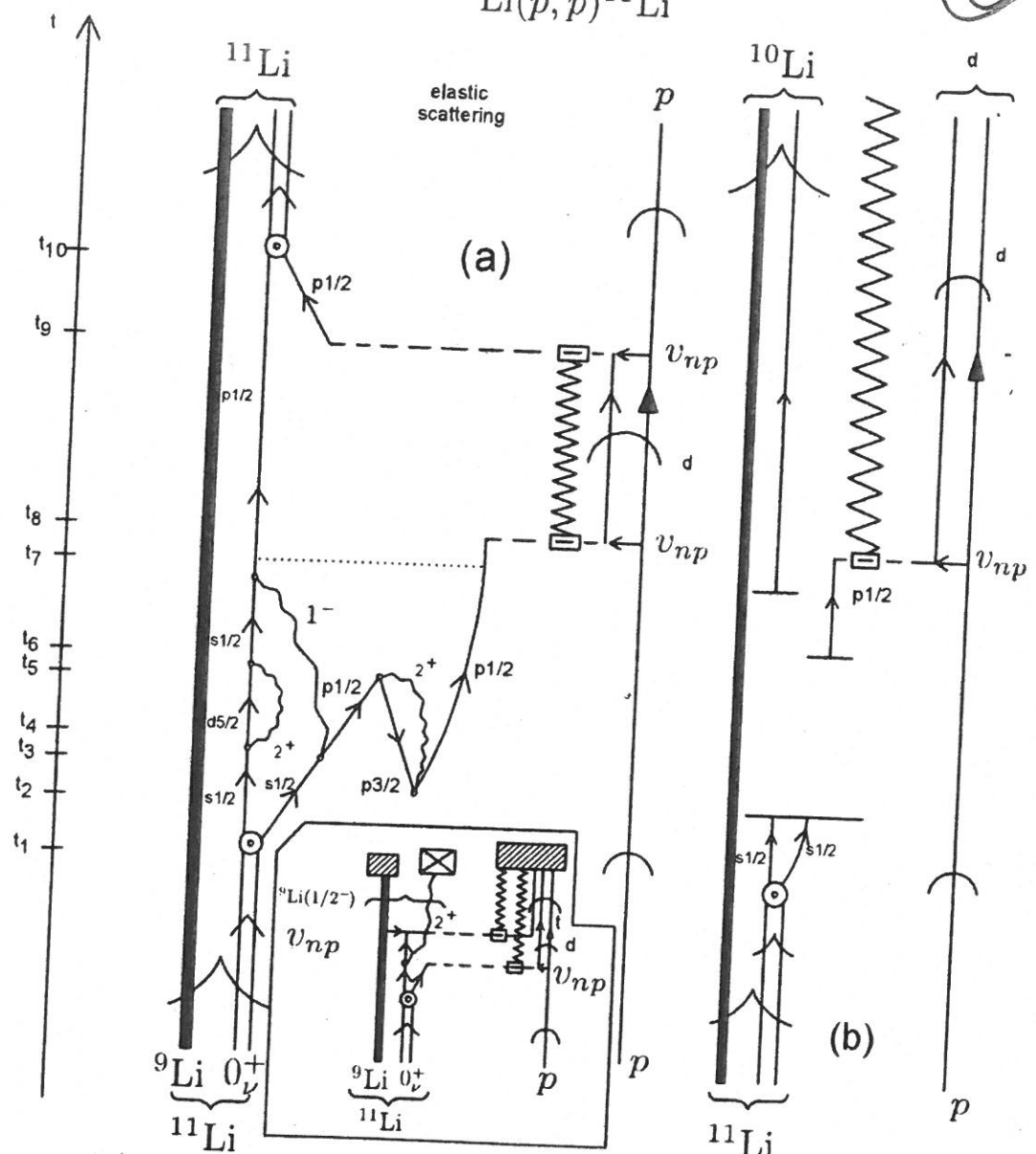
**Fig. 2**

**Figure 2.** NFT representation of the reactions (a)  $^{11}\text{Li}(p, t)^9\text{Li}(\text{gs})$ , (b)  $^{11}\text{Li}(p, t)^9\text{Li}(1/2^-)$ , (c)  $^1\text{H}(^{11}\text{Li}, ^9\text{Li}(\text{gs}))^3\text{H}$  and (d)  $^1\text{H}(^{11}\text{Li}, ^9\text{Li}(1/2^-))^3\text{H}$ . Time is assumed to run upwards. A single arrowed line represents a fermion (proton) ( $p$ ) or neutron ( $n$ ). A double arrowed line two correlated nucleons. In the present case two correlated (halo) neutrons (halo-neutron pair addition mode  $|0\rangle_\nu$ ). A heavy arrowed line represents the core system  $^9\text{Li}(\text{gs})$ . A standard pointed arrow refers to structure, while 'round' arrows refer to reaction. A wavy line represents (particle-hole) collective vibrations, like the low-lying quadrupole mode of  $^9\text{Li}$ , or the (more involved) dipole pygmy resonant state which, together with the bare pairing interaction (horizontal dotted line) binds the neutron halo Cooper pair to the core. A short horizontal arrow labels the proton-neutron interaction  $v_{np}$  responsible for the single-particle transfer processes, represented by an horizontal dashed line. A dashed open square indicates the particle-recoil coupling vertex (for more details see caption to figure F1). The jagged line represents the recoil normal mode (see appendix E discussion connected with figure F1) resulting from the mismatch between the relative center of mass coordinates associated with the mass partitions  $^{11}\text{Li}+p$ ,  $^{10}\text{Li}+d$  (virtual) and  $^9\text{Li}+t$ . It is explicitly drawn as discussed in the text and in appendix F as a mnemonic connected with the particle-recoil coupling vertex. The detector array is represented by a crossed squared box.

The particle detector array  
is represented by a



(17)



neutron pair halo  
 • particle-vibration coupling vertex  
 $\odot$  particle-pair vibration coupling vertex  
 $v_{np}$  proton-neutron int.  
 $\swarrow$  recoil mode

↑ neutron      } bound  
 ↓ proton  
 $2^+ \swarrow$   $^9\text{Li}$  core quadr. vibr. mode  
 $1^- \swarrow$   $^{11}\text{Li}$  giant dipole pygmy resonance mode  
 $\square$  particle-recoil mode coupling vertex

$\uparrow$  deuteron continuum  
 $\downarrow$  proton continuum  
 $\dots$  monopole interaction

Fig. 8

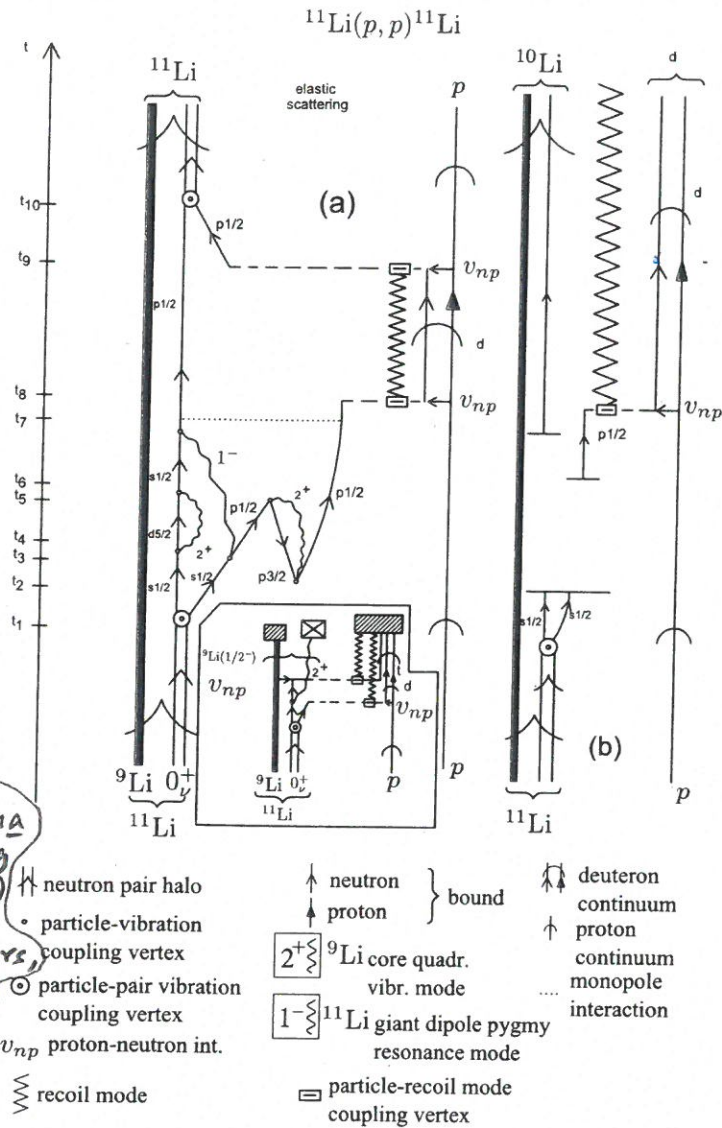


Fig. 8

**Figure 12.** (a) NFT-diagram describing one of the processes contributing to the elastic reaction  $^{11}\text{Li}(p, p)^{11}\text{Li}$  as the system propagates in time (polarization contribution to the global (mean field) optical potential). Processes taking place between  $t_1 - t_7$ : the halo pair addition mode  $|0_\nu^+\rangle$  decays at time  $t_1$  into a pure bare configuration. Its binding to the  $^9\text{Li}$  core is related to parity inversion where the  $s_{1/2}$  continuum orbital is lowered to threshold through cloaking with mainly quadrupole vibrational modes and the  $p_{1/2}$  bound state suffers a strong repulsion into a resonant state by Pauli principle with particles participating in the quadrupole mode. The resulting dressed two-neutron states get bound mainly through the exchange of the  $1^-$  giant dipole pygmy resonance (GDPY), represented for simplicity, as a correlated particle-hole excitation (wavy line labeled  $1^-$ ). The bare pairing interaction (horizontal dotted line acting at  $t_7$ ) contributing subcritically to the binding process (see figure 1(B)). At time  $t_8$ , one of the neutrons of the halo Cooper pair is transferred, with the emission of a recoil mode, to the incoming proton projectile through the proton-neutron interaction  $v_{np}$  (prior representation), leading to a deuteron. This neutron is, at time  $t_9$  transferred back (to virtual  $^{10}\text{Li}$ ) through  $v_{np}$  acting a second time (post representation), with the simultaneous absorption of the recoil mode. Eventually, at time  $t_{10}$  the two neutrons merge, through the particle-pair vibrational coupling, into the halo pair addition mode  $|0_\nu^+\rangle$ . The real part of the diagram contributes to  $U_{\text{opt}}$  while the imaginary one to  $W_{\text{opt}}$ , corresponding to the real and imaginary (absorptive) component of the polarization contribution to the optical potential, arguably to be added to the experimental determined (global)  $^9\text{Li} + p$  elastic scattering optical potential. It is of notice that this diagram provides all the elements to extend and formalize NFT rules of structure so as to be able to deal also with reactions. Within this context see [60], pp 410 and 412 (figures 28 and 29). (b) Same as in (a) up to time  $t_8$  (reason for which no details are repeated between  $t_2$  and  $t_8$ ). From there on the deuteron continues to propagate to the detector (together with the recoil mode). Likely, the neutron in  $^{10}\text{Li}$  will break up before this event. Summing up, in the center of mass reference frame both  $p$  and  $^{11}\text{Li}$  display asymptotic states in entrance as well as in exit channels in case (a), and only in the entrance channel in case (b), while in the exit channel only  $^{10}\text{Li}$  ( $^9\text{Li} + n$ ) and the deuteron do so.

coupling constitutes an essential part of the overall picture developed in nuclei at high rotational frequencies (see [140, 141, 151–157] and references therein; see also e.g. [158] for the coupling to shape vibrations).

### 5.2. Optical potential: example of the $^{11}\text{Li}(p, p)^{11}\text{Li}$ reaction

The discussion carried out in this section is centered around figures 11 and 12. Nuclear field theory in its graphical implementation, allows for a correct description of nuclear structure

## 6.4.4 The structure of "observable" Cooper pairs

(to whom we owe the statistical interpretation of quantum mechanics  
(Born (1964), Pais (1986))

In his Weynflete lectures on Cause and Chance, Max Born states: "... quantum mechanics does not describe an objective state in an independent external world, but the aspect of this world gained by considering it from a certain subjective standpoint, or with certain experimental means and arrangements" (Born (1949), p.100). It is within this context that ~~we are trying~~ <sup>we tried in previous sections</sup> to get insight concerning the structure of nuclear Cooper pairs, <sup>specifically,</sup> in terms of two-nucleon transfer reactions. Being even more subjective (italics) (concrete), we ~~were~~ interested in shedding light on the structure of one of the 5-6 Cooper pairs participating in the condensate (intrinsic state in gauge space) of the Sn-isotopes (ground state rotational band (Potel et al (2013), Potel et al (2017)) through pair transfer processes. That is  $A^{12}_{\text{Sn}}(\text{p.t}) A^{\text{Sn}}_{\text{(gs)}}$  processes in general, and  $^{120}\text{Sn}(\text{p.t}) ^{118}\text{Sn}$  in particular. [Also to learn about the single halo neutron Cooper pair which, bound to the  $N=6$  closed shell system  $^9\text{Li}$  leads to the ground state of  $^{11}\text{Li}$  (Barranco et al (2001)). In this case making use of the reaction  $^1\text{H}(^{11}\text{Li}, ^9\text{Li}(\text{gs})) ^3\text{H}$  (Tanihata et al (2008), Potel et al (2010)).]

subject

do not write

[ 7. no es necesario para el libro  
si el articulo no está pronto  
en tiempo.

From a strict observational perspective, concerning Cooper pairs, one can only refer to the information two-nucleon transfer absolute differential cross sections carry on these entities.

On the other hand, leaving ~~out~~ to a future publication the discussion regarding the microscopic calculation of the optical potential, the carriers mediating information between structure and differential cross sections, e.g. between target and outgoing particle in a standard laboratory setup, are the distorted waves [associated with initial and final channels]. These functions can be studied independently of the transfer processes under consideration, in elastic scattering experiments. Consequently, the non-local, correlated formfactors,

$$F(\vec{r}_1, \vec{r}_2, \vec{r}_{Ap}) = F_{\text{succ}} + F_{\text{sim}} + F_{\text{NO}}, \quad (1)$$

Sum of the successive and simultaneous transfer processes and of the non-orthogonality correction, calculated with different sets of two-nucleon spectroscopic amplitudes can be compared at profit to each other. This is in keeping with the fact that they can be related, in an homogeneous fashion, with the absolute cross sections or, better, with the square root of these quantities.

~~Once the stability, theoretical  
we go to  $^{11}\text{Li}$ .~~

Koblenz 6/8/17

(20)

Examples of (1) for the reaction  $^{120}\text{Sn}(\text{p}, \text{t})^{118}\text{Sn}(\text{gs})$  calculated making use of  $\beta$ -coefficients associated with BCS, HFB and NFT+(NG) theoretical descriptions, are displayed in Fig. 1, for a representative value of the  $\vec{r}_{\text{PA}}$  incident proton relative coordinate. A quantitative assessment of the differences between the predictions of the different models can be made with the help of the root mean square deviation (RMSD) taken as reference the NFT+(NG) results. The differences, normalized with respect to the mean square radius  $\langle r^2 \rangle^{1/2} = \sqrt{\frac{3}{5}} R_0$  ( $\approx 4.6 \text{ fm}$ ) amount to few percent (%) (percent (%)) Table  $\Sigma'$ ). As expected, much smaller than those related to  $\sigma$  and closely connected with the estimates provided by the square root differences of the absolute cross sections  $\sigma_{\text{abs}}$  (Table II). See also "the section on simple estimates for RMSD of  $F(\vec{r}_1, \vec{r}_2, \vec{r}_{\text{PA}})$ ".

→ [Having assessed the stability of the quantity (1) we discuss in what follows the single halo Cooper pair of  $^{11}\text{Li}.$ ]

(regarding structure inputs)

do not write

see comment

P. ① (ahura) (18)

Kob. 5/8/17

Caption to Tables  $\Sigma$ ,  $\Pi$ ,  $\Omega$ ,  $\Theta$  of pp (21) and

(22)

(20)<sub>a</sub>

### Table $\Sigma$

Simple estimates of the RMSD associated with different approximations to calculate  $F(\vec{r}_1, \vec{r}_2, \vec{r}_{AP})$  associated with the reaction  $^{120}\text{Sn}(\text{pit})^{118}\text{Sn}(\text{gs})$  and referred to the empirical values related to  $\sigma_{\text{exp}}$ .  
Table  $\Sigma'$ , same as Table  $\Sigma$  but using  $\sigma_{\text{exp}}$   
Table  $\Pi$

Relative deviations of the absolute cross section (amplitudes) referred to experimental value, associated with different structure models used to calculate the two-nucleon transfer spectroscopic amplitudes, associated with the reaction  $^{120}\text{Sn}(\text{pit})^{118}\text{Sn}(\text{gs})$

Same as in Table  $\Pi$  but regarding the superfluid order parameter  $\alpha_0$ . The ansatz has been made that one can define an empirical (effective) value of  $\alpha_0$  connected with experiment according to  $(\alpha_0)^2_{\text{emp}} / (\alpha_0)^2_{\text{NFT}} = \sigma_{\text{exp}} / \sigma_{\text{NFT}} = 2250 / 2097 = 1.073$ . That is

$(\alpha_0)^2_{\text{emp}} = 29.13$ . Thus  $(\alpha_0)_{\text{emp}} = 5.4$ . The relative error can be estimated as  $(\sum \Delta (\alpha_0^2)_{1/2})^{1/2} / 3$  i.e. 1.71, resulting in  $(\alpha_0)_{\text{emp}} = 5.4 \pm 32\%$ .

Likely a better simple estimate of RSMD of  $F(\vec{r}_1, \vec{r}_2, \vec{r}_3)$  (5)

	$\sqrt{\sigma} (\mu b)^{1/2}$	$ \sqrt{\sigma_{\text{exp}}} - \sqrt{\sigma_i}  \times 10^{-2} \text{ fm}$	$\frac{ \sqrt{\sigma_{\text{exp}}} - \sqrt{\sigma_i} }{r^{27/2}} \text{ (%)}$
exp	47.43	—	—
BCS	49.55	2.12	0.46
HFB	44.22	3.21	0.70
NFT+(NG)	45.79	1.64	0.36

$$\sqrt{\mu b} = 10^{-2} \text{ fm}$$

Table 4.  $\Sigma$

# Simple estimates for RSMD of $F(\vec{r}_1, \vec{r}_2, \vec{r}_{AP})$

Kofb. 6/18/17

(4) (21)

Table Σ

$i$	$\sigma (\mu b)$	$ \sigma_{exp} - \sigma_i  (\mu b)$	$\sqrt{\sigma_{exp} - \sigma_i} fm$	$\sqrt{\sigma_{exp} - \sigma_i} / \langle r^2 \rangle^{1/2} (\%)$
exp	2250	0	—	—
BCS	2455	205	0.14	3
HFB	1955	295	0.17	4
NFT+(NG)	2097	153	0.12	3

$$\mu b = 10^{-6} \times 10^2 fm; \sqrt{\mu b} = 10^{-2} fm$$

NFT+(NG)

$$"RMSD" = \sqrt{|\sigma_{exp} - \sigma_{NFT}|} = \sqrt{153 \mu b} = 12.4 \times 10^{-2} fm$$

$$R_0 = 1/2 A^{1/3} fm \approx 5.9 fm \quad \langle r^2 \rangle^{1/2} = 0.12 fm \quad \frac{3}{5} R_0 = 4.6 fm$$

"RMSD" Root Mean Standard Deviation  
with respect to an imaginary  $F(\vec{r}_1, \vec{r}_2, \vec{r}_{AP})$   
associated with experiment.

Table II

BCS

$$"RMSD" = \sqrt{205 \mu b} = 14.3 \times 10^{-2} fm = 0.14 fm; \frac{0.14}{5.9} = 0.02$$

HFB

$$"RMSD" = \sqrt{295 \mu b} = 0.17 fm; \frac{0.17}{5.9} = 0.029$$

Arguments with  $\alpha_0$

Ansatze

$$\sigma \propto \alpha_0^2$$

$$(\alpha_0)_{emp} \approx 5,3972$$

$$\frac{(\alpha_0)_{emp}^2}{(\alpha_0)_{NFT}^2} = \frac{\sigma_{exp}}{\sigma_{NFT}} = \frac{2250}{2097} = 1.073; (\alpha_0)_{emp}^2 = 1.073 \times (5.21)^2 = 29.13$$

~~do not type~~

	$\alpha_0$	$(\alpha_0)^2$	$\Delta(\alpha_0)_i^2 =  (\alpha_0)_{emp} - (\alpha_0)_i^2  (\sqrt{-})$	$(\Delta(\alpha_0)_i^2 / (\alpha_0)_{emp}^2)^{1/2} (\%)$
Temp	5,3972	29.13	—	—
BCS	5,74	32,95	3,91 (1.98)	13
HFB	5,09	25,91	3,13 (1.77)	11
NFT	5,21	27,14	1,90 (1.38)	7

Table S2

some air  $\Theta$

me  $\Theta$

~~Summing up,~~

Typical deviations between theory and experiment (empirical) results, as well as between different models among themselves is considerably smaller for  $F(\vec{r}_1, \vec{r}_2, \vec{r}_{AP})$  than for  $\alpha_0$ .

A simple estimate is given by

$$\langle r^2 \rangle^{1/2} \pm \sqrt{10\sigma_{exp} - \sigma_{cl}} \approx 4.6 \pm 0.14 \text{ fm}$$

i.e.  $\langle r^2 \rangle^{1/2} \pm 3\%$

and

$i$	$[(\alpha_0)_i \pm (\Delta(\alpha_0^2))_i^{1/2}]$	$(\Delta(\alpha_0^2))_i^{1/2} / (\alpha_0)_i (\%)$
BCS	$5.74 \pm 1.98$	34
HFB	$5.09 \pm 1.77$	35
NFR(NG)	$5.21 \pm 1.38$	26

i.e., Table (1)

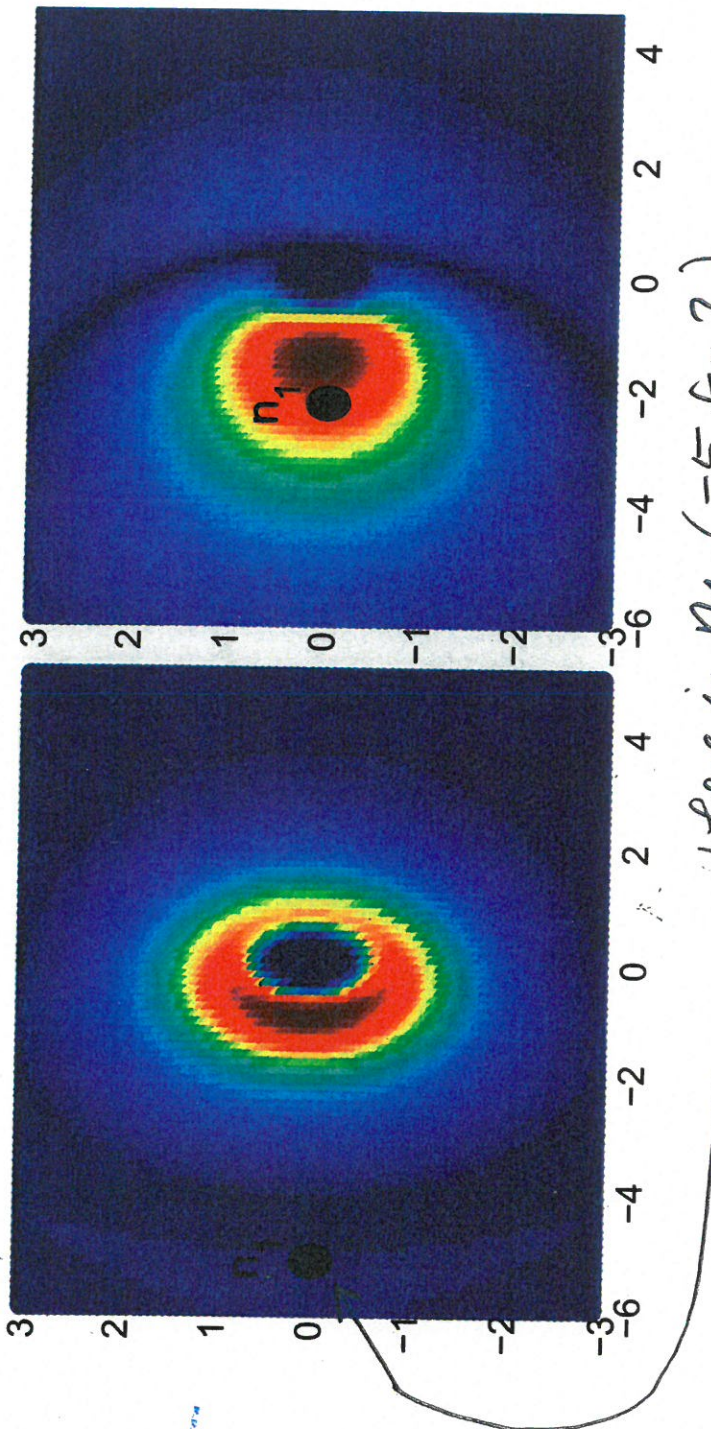
$$(\alpha_0)_{em} \pm \langle (\Delta(\alpha_0^2))_i^{1/2} / (\alpha_0)_i \rangle$$

$$\approx 5.4 \pm 32\%$$

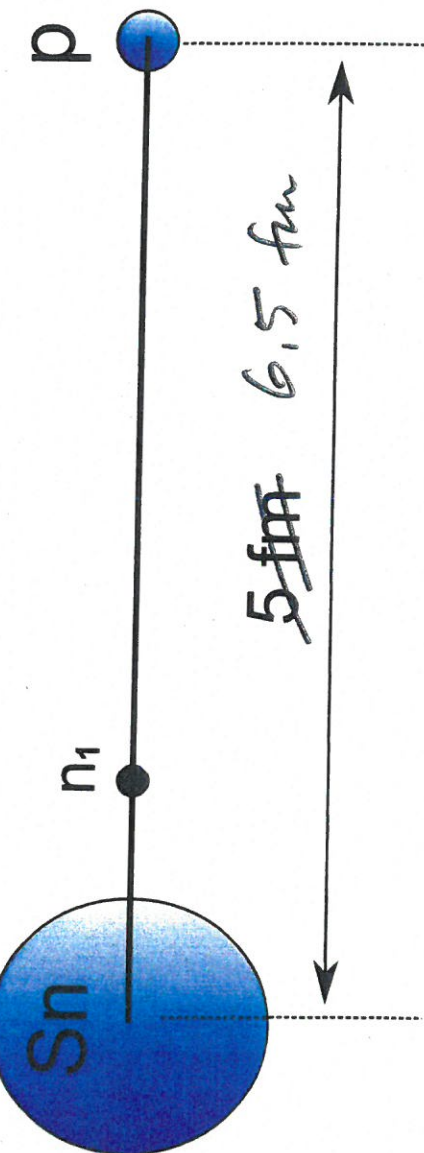
Class

# Non-local, correlated form factor

$$F(\mathbf{r}_1, \mathbf{r}_2, \mathbf{r}_{A\rho}) = \phi_f(\mathbf{r}_{\rho 1}, \mathbf{r}_{\rho 2}) V_{pn}(\mathbf{r}_{\rho 1}) V_{pn}(\mathbf{r}_{\rho 2}) \phi_i(\mathbf{r}_{A1}, \mathbf{r}_{A2})$$



Where is  $n_1$  (-5 fm?)



$$\begin{aligned} R_0 &= 6 \text{ fm} \\ \alpha &= 0.65 \\ 6.5 \text{ fm} &\approx R_0 + \alpha \\ {}^{120}\text{Sn} \end{aligned}$$

Fig. 1. Form factor associated with the reaction  ${}^{120}\text{Sn}(\text{pit}) {}^{118}\text{Sn}(\text{gr})$  for a fixed value of  $\mathbf{r}_{PA} (= 5 \text{ fm})$  and of  $r_{n_1}$  ( $= -2 \text{ fm}$  and  $-6 \text{ fm}$ ) as a function of the  $x, y$  coordinates of  $n_2$ .

colour  
scale  
gregory

## References

(24) 6

M. Born, Natural philosophy of cause and chance, Oxford University Press, Oxford (1949)

Nobel Lecture (1954)

M. Born, The statistical interpretation of quantum mechanics, Nobel Lectures, Physics 1942-1962, Elsevier, Amsterdam, 256 (1964)

A. Pais, Inward bound, Oxford University Press, Oxford, 255 (1986)

G. Potel, A. Indini, F. Barranco, E. Vigezzi and R. A. Broglia, Quantitative study of coherent pairing modes with two-neutron transfer: Sn isotopes, Phys. Rev. C 87, 054321 (2013)

G. Potel, A. Indini, F. Barranco, E. Vigezzi and R. A. Broglia, From bare to renormalized order parameter in gauge space: structure and reactions, Phys. Rev C (in press) (2017).

I. Tanihata .... Measurement..., Phys. Rev. Lett. 100, 192502 (2008)

G. Potel, F. Barranco, E. Vigezzi and R. A. Broglia, Evidence for phonon mediated pairing interaction in the halo nucleus  $^{11}\text{Li}$ , Phys. Rev. Lett. 105, 172502 (2010)

F. Barranco, P. F. Bortignon, R. A. Broglia, G. Colò and E. Vigezzi, The halo of the exotic nucleus  $^{11}\text{Li}$ : a single Cooper pair, Eur. Phys. J. A 11, 385 (2001).

## 6.4.5 Closing the circle<sup>11)</sup>

(25) -di

(12)  
\*\*

In the first reference of this monograph<sup>11)</sup>

~~(Born 1926a)~~ entitled "Quantum mechanics of collision phenomena", Born considers the elastic scattering of a beam consisting of  $N$  electrons which cross unit area per unit time, scattered by a

static potential. The stationary wavefunction describing the scattering process behaves asymptotically as,

$$e^{ikz} + f(\theta, \phi) \frac{e^{ikr}}{r} \quad (k = \frac{mv}{\hbar})$$

The number of particles scattered into the solid angle  $d\Omega = \sin\theta d\theta d\phi$  is given by  $N |f(\theta, \phi)|^2 d\Omega$ . To connect with Born notation one has to replace  $f(\theta, \phi)$  by  $\Phi_{mn}$ , where  $n$  denotes the initial-state plane wave in the  $z$ -direction and  $m$  the asymptotic final-state in which the

<sup>11)</sup>\*\* In this section we follow closely Pais (1986) pp. 256-258.

<sup>12)</sup>\* Born (1926a)

26

wave move in the direction fixed by the angles  $(\theta, \phi)$ . Then Born writes that  $\Phi_{mn}$  determines the probability for the scattering of the electron from the z- to the  $(\theta, \phi)$ -direction, adding a footnote in proof, as already mentioned, stating that a more precise consideration shows that the probability is proportional to the square of  $\Phi_{mn}$ . In a second paper with the same title of the first he states explicitly that the probability is to be connected with the modulus squared, <sup>13</sup>\*. Within this context, the matrix element between the entrance and exit channel distorted waves of  $F(\vec{r}_1, \vec{r}_2, \vec{r}_{AP})$  is proportional to  $f(\theta)$  and thus,  $\Phi_{m,n}$ .  $F$  is not directly measurable (~~directly~~), but the closer one can come of a theoretical construct connecting Cooper pair (s+r) <sup>14</sup>\*\*.

<sup>14</sup>\*\*) The motion of particles follows probability laws but the probability itself propagates according to the law of causality. And concerning the distinction between classical and quantal probability he states: "the classical theory introduces the microscopic coordinates which determine the individual processes only to eliminate them because of ignorance by averaging over their values; whereas the new theory get the same results without introducing them at all... We free the forces of their classical duty of determining directly the motion of particles and allow them instead to determine the probability of states".

<sup>13</sup>\*) Born 1926b

M. Born, Quantenmechanik der Stoßvorgänge, Zeitschr. f. Phys.,  
38: 803 (1926)

and experiment. Because this construct does not change much with the theory one uses to calculate the spectroscopic two-nucleon transfer amplitudes for nuclei lying along the stability valley, is provided, all display ODLRD<sup>15</sup> that the associated absolute cross sections are rather stable, and do provides a natural order parameter to measure deformation in gauge space (number of Cooper pairs participating in the condensate).

On the other hand, in the case of halo, weakly bound exotic nuclei like  $^{11}\text{Li}$ , the sensitivity of the absolute cross sections to the models used to calculate  $F(\vec{r}_1, \vec{r}_2, \vec{r}_{PA})$  is stronger, and directly related to the conspicuous change which renormalization produces in the radial shape of the single-particle wavefunctions of the halo.

(15) neutrons forming the Cooper pair.

from  
to review  
index

Use Rho-m and two sp pots, one for 1s and one for 1p  
ala G. Bertsch.

A result directly related to the fact that the nucleus is a finite many-body system<sup>(16)\*</sup>, where surface effect play a central role<sup>\*\*</sup>, light halo weakly bound exotic nuclei like  $^{11}\text{Be}$  and  $^{11}\text{Li}$  being paradigm<sup>\*\*</sup> of these leptodermic properties.

Within this context, self-consistency in  $(\text{NFT})_{\text{ren}}$  implies both the renormalization of single-particle energies and occupancies ( $E_j, z_j(\omega)$ ), as well as of radial wavefunctions ( $\tilde{\Phi}(r)^{(i)}$ ). For each  $E_j$  there can be more than one radial function, depending on whether the nucleon is moving around the ground state ( $i = \text{gs}$ ) or an excited state ( $i = \text{coll}$ ) of the core. In keeping with the fact that  $\tilde{\Phi}(r)^{(i)}$  are the formfactors associated with transfer processes, self-consistency in  $(\text{NFT})_{\text{ren}}$  is ultimately related to unification of  $(s+r)$ .

\*\*) One could be tempted to say, caricatures.

(16)\*) Within this context see Broglia (2002) and refs. therein

R.A.Broglia, The surfaces of compact systems: from nuclei to stars, Surface Science 500, 759 (2002).

20/8/17

This makes it possible to study, among other things, renormalization effects in terms of individual quantum states, and pairing correlations resulting from bare plus induced  $^3S_0$  interactions in systems with few (5-6) Cooper pairs (superfluid nuclei) down to a single Cooper ( $^{11}\text{Li}$ ),

\*  
29